EBioMedicine 38 (2018) 113–126

Contents lists available at ScienceDirect

EBioMedicine

journal homepage: www.ebiomedicine.com

EBioMedicine
Published by THE LANCET

Research paper

SRSF1 modulates PTPMT1 alternative splicing to regulate lung cancer cell radioresistance

Junxiu Sheng [a,1], Qingzhi Zhao [b,1], Jinyao Zhao [b,1], Wenjing Zhang [b,*,1], Yu Sun [b], Pan Qin [c], Yuesheng Lv [b], Lu Bai [b], Quan Yang [b], Lei Chen [b], Yangfan Qi [b], Ge Zhang [d], Lin Zhang [b], Chundong Gu [g], Xiaoqin Deng [a], Han Liu [b], Songshu Meng [b], Hong Gu [c], Quentin Liu [b], Judy M. Coulson [e], Xiaoling Li [f], Bing Sun [g,**], Yang Wang [b,*]

[a] Department of Radiation Oncology, First Affiliated Hospital, Dalian Medical University, Dalian 116044, China
[b] Institute of Cancer Stem Cell, Dalian Medical University, Dalian 116044, China
[c] Faculty of electronic information and electrical engineering, Dalian university of Technology, Dalian 116001, China
[d] Department of Immunology, Dalian Medical University, Dalian 116044, China
[e] Cellular & Molecular Physiology Department, University of Liverpool, UKL69 3BX, UK
[f] Signal Transduction Laboratory, NIEHS, RTP, NC 27709, USA
[g] Department of Thoracic Surgery, First Affiliated Hospital, Dalian Medical University, Dalian 116044, China

ARTICLE INFO

Article history:
Received 11 September 2018
Received in revised form 31 October 2018
Accepted 2 November 2018
Available online 11 November 2018

Keywords:
Alternative splicing
SRSF1
PTPMT1
AMPK
Radio-resistance

ABSTRACT

Background: Radioresistance is the major cause of cancer treatment failure. Additionally, splicing dysregulation plays critical roles in tumorigenesis. However, the involvement of alternative splicing in resistance of cancer cells to radiotherapy remains elusive. We sought to investigate the key role of the splicing factor SRSF1 in the radioresistance in lung cancer.

Methods: Lung cancer cell lines, xenograft mice models, and RNA-seq were employed to study the detailed mechanisms of SRSF1 in lung cancer radioresistance. Clinical tumor tissues and TCGA dataset were utilized to determine the expression levels of distinct SRSF1-regulated splicing isoforms. KM-plotter was applied to analyze the survival of cancer patients with various levels of SRSF1-regulated splicing isoforms.

Findings: Splicing factors were screened to identify their roles in radioresistance, and SRSF1 was found to be involved in radioresistance in cancer cells. The level of SRSF1 is elevated in irradiation treated lung cancer cells, whereas knockdown of SRSF1 sensitizes cancer cells to irradiation. Mechanistically, SRSF1 modulates various cancer-related splicing events, particularly the splicing of PTPMT1, a PTEN-like mitochondrial phosphatase. Reduced SRSF1 favors the production of short isoforms of PTPMT1 upon irradiation, which in turn promotes phosphorylation of AMPK, thereby inducing DNA double-strand break to sensitize cancer cells to irradiation. Additionally, the level of the short isoform of PTPMT1 is decreased in cancer samples, which is correlated to cancer patients' survival.

Conclusions: Our study provides mechanistic analyses of aberrant splicing in radioresistance in lung cancer cells, and establishes SRSF1 as a potential therapeutic target for sensitization of patients to radiotherapy.

1. Introduction

Radiotherapy is one of the most effective approaches for cancer therapy. Some complicated biological processes are involved in radiotherapy to induce cancer cell death [1,2]. Nevertheless, many cancer patients develop resistance to radiotherapy during treatment, which may be caused by different factors [3–5]. However, the underlying mechanisms of the radioresistance development are still elusive.

>95% of human genes undergo alternative splicing (AS) to generate protein diversity [6]. As one of the most important mechanisms of gene regulation, AS plays critical roles in modulating protein function intricately. In addition, AS is tightly regulated in different tissues and

Abbreviations: SRSF1, Serine/arginine-rich Splicing Factor 1; SR proteins, Serine/arginine-rich proteins; NMD, nonsense-mediated decay; PTPMT1, Protein Tyrosine Phosphatase, Mitochondrial 1; AS, Alternative Splicing; AMPK, AMP-activated Protein Kinase; γH2AX, gamma-Histone H2AX; Chk2, Checkpoint kinase 2; IR, ionizing radiation; EMT, epithelial to mesenchymal transition.

* Correspondence to: W. Zhang and Y. Wang, Institute of Cancer Stem Cell, Dalian Medical University, Dalian 116044, China.
** Correspondence to: B. Sun, Department of Thoracic Surgery, First Affiliated Hospital, Institute of Cancer Stem Cell, Dalian Medical University, Dalian, 116044, China.
E-mail addresses: zhangwj@dmu.edu.cn (W. Zhang), dysunbing@163.com (B. Sun), yangwang@dmu.edu.cn (Y. Wang).
[1] These authors contributed equally to this work.

https://doi.org/10.1016/j.ebiom.2018.11.007

Research in context

Evidence before this study

Splicing dysregulation plays critical roles in tumorigenesis. Radioresistance is the major cause of cancer treatment failure. However, the involvement of alternative splicing in resistance of cancer cells to radiotherapy remains elusive.

The value of this study

This study aimed to investigate whether the splicing factor SRSF1 is involved in radioresistance in lung cancer. We found that the splicing of PTPMT1 is modulated by SRSF1. The splicing switch towards the short isoform of PTPMT1 leads to the increased phosphorylation of AMPK, which sensitizes lung cancer cells to radiotherapy.

Implications of all the available evidence

Our study provides mechanistic analyses of deregulated splicing in radioresistance in lung cancer, and establishes SRSF1 as a potential therapeutic target for sensitization of patients to radiotherapy.

developmental stages, and commonly controlled by various splicing factors, including serine/arginine-rich (SR) proteins. Importantly, deregulation of AS can lead to cancer [7–10]. Certain splicing isoforms of cancer related genes can function as molecular markers of cancer [11], or directly regulate cancer initiation and progression [12].

Aberrant expression of splicing factors is one of the main causes of splicing deregulation in cancer [13–16]. For example, the splicing factor SRSF1 is a crucial family member of SR proteins. SRSF1 usually binds to exonic splicing enhancers to promote splicing, however it binds to intronic elements to inhibit splicing [17,18]. In addition to splicing regulation, SRSF1 was also reported to participate in multiple biological functions, including translation control, nonsense-mediated RNA decay (NMD), RNA transport, and senescence [19–22]. SRSF1 can interact with translating ribosomes and promote translation [23]. Moreover, the mRNA translational targets of SRSF1 were systematically identified to be involved in cell cycle regulation [24]. SRSF1also increases the binding of NMD factor UPF1 to mRNAs, thereby bypassing UPF2 recruitment and promoting NMD [25].In addition, SRSF1 stabilizes p53 through blocking its MDM2-dependent proteasomal degradation, thus to result in oncogene-induced senescence (OIS) [22]. Strikingly, SRSF1 has been identified as a potential oncogene that is overexpressed in several cancers [26–28]. The elevated expression of SRSF1 results, in cooperation with MYC, in the transformation of mammary epithelial cells [28]. Moreover, SRSF1 regulates the epithelial-to-mesenchymal transition (EMT) through modulating the splicing of Ron proto-oncogene [29], as well as controls the alternative splicing of PRRC2C and MKNK2 to regulate lung cancer progression [28,30].Most importantly, SRSF1 regulates the splicing of BIM to inhibit imatinib-induced apoptosis, thereby conferring cancer cells resistance to imatinib [31]. In addition, other splicing factors, such as hnRNP A1 and PTB, have been reported to influence pyruvate kinase splicing and cell metabolism to affect tumorigenesis [32], whereas RBM4 controls the alternative splicing of Bcl-x to inhibit lung cancer progression [14]. Therefore, specifically targeting deregulated AS may provide a novel avenue for cancer therapy [33].

In this study, we screened splicing factors that might participate in radioresistance regulation, and found levels of SRSF1 is markedly increased in radioresistant cells. In addition, increased levels of SRSF1 are examined in lung cancer cells that are treated with ionizing radiation, suggesting that SRSF1 might play key roles in radioresistance in lung cancer. Meanwhile, depletion of SRSF1 could significantly induce DNA damage, and apoptosis of cancer cells upon irradiation. Mechanistically, knockdown of SRSF1 favors the production of short isoforms of PTPMT1, thereby inducing the phosphorylation of AMPK and sensitizing cancer cells to radiotherapy. Our study highlights the importance of SRSF1 as a potential therapeutic target to sensitize cancer patients for radiotherapy.

2. Materials and methods

2.1. Cell culture and transfection

All cell lines used in our study were purchased from American Type Culture Collection (Manassas, VA, USA). The human embryonic kidney HEK293T (Cat# CRL-11268, RRID: CVCL_1926) cells were maintained in DMEM (high glucose) medium with 10% fetal bovine serum (FBS, Hyclone) and 1% penicillin/streptomycin (P/S), in humidified 5% CO_2 at 37 °C. The human non-small lung carcinoma cell line A549 (Cat# CRM-CCL-185, RRID: CVCL_0023) was maintained in F-12 K medium with 10% FBS and 1% P/S, in humidified 5% CO_2 at 37 °C. The H1299 (Cat# CRL-5803, RRID: CVCL_0060) human lung carcinoma cells were cultured in RPMI-1640 medium containing 10% FBS and 1% P/S, in humidified 5% CO_2 at 37 °C.

To generate H1299 and A549 cell lines stably knocking-down SRSF1, lentiviral particles were produced by transient transfection of HEK 293 T cells with pLKO-SRSF1-sh1 or pLKO-SRSF1-sh2 or pLKO-empty vectors according to manufactures protocols. 72 h after transfection, the supernatant media containing lentivirus was collected and incubated with H1299 and A549 cells for 24 h in normal medium containing 8 μg/mL Polybrene (Sigma). Then stably integrated cells were selected by 5 μg/mL puromycin for one week. All cell lines were confirmed by western blots before further analysis.

To stably express PTPMT1A or PTPMT1B in H1299 cells, we used lentiviral vectors as well. Briefly, HEK293T cells were transiently transfected with pCDH-HA-PTPMT1A or pCDH-HA-PTPMT1B or pCDH-HA-empty vectors according to manufactures protocols. The supernatant media containing lentivirus was collected and used to infect H1299 cells, followed by 5 μg/mL puromycin selection for one week. The stable expression cell lines were confirmed by western blots before further analysis.

To determine the localization of PTPMT1A or PTPMT1B, we transfected 1 μg of HA-tagged PTPMT1A or PTPMT1B vectors in H1299 cells using lipofectamine 3000 according to the manual. 48 h later, H1299 cells were fixed for further immunofluorescence analysis.

In order to examine the effect of over-expression of SRSF1 on PTPMT1 splicing changes, we co-transfected 0.2 μg of PTPMT1 minigene reporters with 0.4 μg of SRSF1 using lipofectamine 3000 according to the manual. Cells were collected for further analysis of RNA level at 48 h after transfection.

2.2. Splicing reporter constructs

To construct the PTPMT1 reporter, the fragment containing exon 2, part of intron 2, exon 3, part of intron 3, and exon 4 of PTPMT1 were cloned into *EcorI* and *Not*I sites of pCDNA3.1(+) vector. To mutate SRSF1 binding sites of PTPMT1 reporters, overlapping PCR was used with different paired primers. The primers used for plasmid construction were listed in Supplemental Table 1.

2.3. Real-time cell analysis (RTCA) experiments

Cell proliferation assays were performed using xCELLigence Real-Time Cell Analyzer RTCA-MP system (Acea Biosciences/Roche Applied Science). Add 50 uL RPMI 1640 media with 10% FBS to each well of *E*-Plate 96 (Roche Applied Science) to obtain equilibrium. H1299 cells

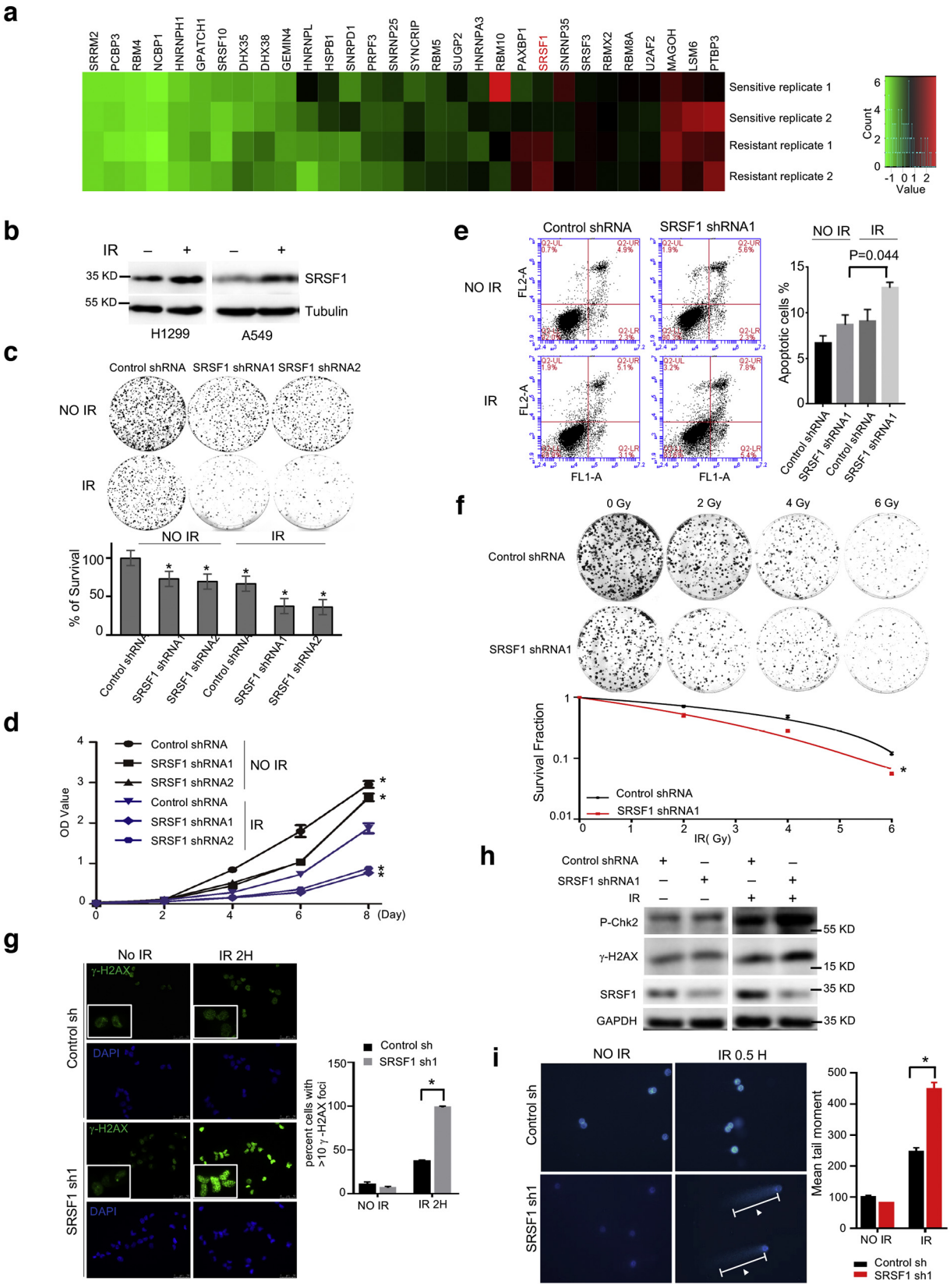

transfected PTPMT1 B were collected and the concentration of the cell suspensions were adjusted to 2×10^4 cells/mL. Add 100 μL of cell suspension to each well of E-Plate 96. Impedance readings were taken automatically every 15 min until the end of the experiment and plotted as Cell Index ± SD.

2.4. Cell proliferation assay

H1299-SRSF1-sh cells and control cells were seeded in 96-well plates at 1000 cells per well and grown for 8 days. Cell numbers were measured using CCK-8 (Beyotime) at 0, 2, 4, 6 and 8 day after incubation.

2.5. Assay of splicing with semi-quantitative RT-PCR

The total RNAs were extracted from transfected cells using TRIzol reagent (Invitrogen) according to the manufacturer's protocol. Genomic DNA were removed by 1 h DNase I (Invitrogen) treatment at 37 °C. Total RNA (2 μg) was then reverse-transcribed into cDNA with SuperScript III (Invitrogen) using poly T primer, and one-tenth of the resulting cDNA was used as the template for PCR amplification (25 cycles of amplification). RT-PCR products were separated on 3% agarose gels, and imaged were captured using a CCD camera (Tanon 2500R). The quantification of mRNA isoforms was achieved by comparison of the integrated optical density of detected bands measured by the GIS 1D Gel Image System (ver. 4.2; Tanon).

2.6. Western blot

Cells were washed twice with cold PBS and then lysed in lysis buffer (50 mM HEPES, 150 mM NaCl (4.38 g), 1 mM EDTA, 1% (w/v) CHAPS and Sigma protease inhibitor cocktail). The cell lysates were centrifuged at 12000 rpm for 15 min and the protein concentration was measured using Coomassie protein assay kit. Equal amounts of total protein were resolved by 10% SDS-PAGE and transferred to nitrocellulose membrane. All primary antibodies were diluted 1000 times for WB if not specified. The following antibodies were used in this study: SRSF1 (#sc-33,652, RRID: AB_628248) antibody was purchased from SCBT. Anti-HA tag antibody (#mms-101p-1000, RRID: AB_291259) were purchased from Convance. Alpha-tubulin (#T5168, RRID: AB_477579, 1:5000 dilution) was purchased from Sigma-Aldrich. Bound antibodies were visualized with the ECL kit (GE Healthcare).

2.7. Assay of SRSF1 expression with Realtime PCR

We performed the real-time PCR using the Maxima SYBR Green qPCR Master Mix (Thermo Scientific) and a 7500 real-time PCR system (Life Technologies) according to manufacturer's instructions. The expression level of SRSF1 was normalized to the endogenous expression of GAPDH.

2.8. Heat map

We kept genes: i) FPKM (Fragments Per Kilobase of transcript per Million mapped reads) values of one gene are not equal in all samples; ii) At least one of the FPKM values in all samples is larger than or equal to 3; iii) The ratio of maximum FPKM value and minimum FPKM value in all samples is larger than or equal to 2. The log 2 ration of FPKM values of kept genes which normalized by the FPKM value of control sample were used as input of Cluster 3.0 (de Hoon, et al., 2004). Then we used hierarchical clustering method based on Pearson correlation with average linkage to cluster the dataset, and further viewed the results with Java TreeView. We selected the cluster in this pattern regulated by SRSF1 with or without ionizing radiation as our target dataset.

2.9. Ionizing radiation treatment

H1299-SRSF1-sh cells or control cells grown on 10 cm plates with liquid culture media were irradiated with ionizing radiation using an X-RAD 320ix Biological Irradiator (Precision X-ray Inc.). The cells were treated 50 cm from the source of radiation (SSD) with a dose of 6 Gy. The cells were treated at room temperature.

2.10. Colony formation assay

H1299 cells (or A549 cells) knocking-down SRSF1 or expressing PTPMT1A, PTPMT1B, and control vectors (1000 cells per dish) were grown in the 10-cm dishes and incubated at 37 °C in humidified incubator for 9 days. Colonies were fixed with methanol at room temperature and stained with crystal violet followed by washing with water and photographed.

2.11. Mouse irradiation study

H1299 cells stably expressing PTPMT1B or control (1×10^6) were suspended in 100 μL of PBS and were injected subcutaneously into the abdomen side of 6-week-old BALB/c nude mice. Macroscopic observation and tumor volume measurements were performed every 3 days. When tumors reached the volume of approximately 250mm^3, the mice (six per treatment group) were exposed to 6 Gy radiation. After IR, tumor volume measurements were performed every 2 days. Tumor volume was calculated according to the following formula: tumor volume (mm^3) = length (mm) × (width (mm))^2/2. The body weight during the course of the study were measured every 3 days or 2 days. All animals were sacrificed 40 days after injection and excised tumors were weighed. The animal experiments were strictly compliant with the animal care guidelines of Dalian medical university.

2.12. Clinical tissues samples collection

We collected fresh lung cancer tissues and adjacent normal tissues from patients with pathologically and clinically confirmed lung carcinomas. All human tumor tissues were obtained with written informed consent from patients or their guardians prior to participation in the study. Use of the tumor specimens in this study was approved by the Institutional Review Board of the Dalian Medical University. All of tissue specimens were immediately frozen in liquid nitrogen and kept at −80 °C until the extraction of protein or mRNA.

2.13. High throughput mRNA-sequence and data analysis

Total RNAs of H1299 cells stably knocking-down SRSF1, and control vectors with or without treatment of ionizing radiation were isolated using Trizol™ method and subsequently cleaned using RNAeasy Kit (Qiagen). The DNA was removed from total RNAs by digesting in column with RNAse free DNAse according to manufacturer's instruction. Illumina TruSeq Total RNA Sample Prep kits were used to further purify polyadenylated RNA from total RNA. Ribosomal RNA was removed by Epicentre Ribo-zero™ rRNA removal Kit (Epicentre, USA). RNA-seq

Fig. 1. Reduction of SRSF1 sensitizes lung cancer cells to IR. (a) Heat map depicting gene expression of splicing factors in radiosensitive and radioresistant cancer cells. (b) The protein level of SRSF1 was examined in H1299 and A549 cells that were treated with or without IR. (c) Colony formation assays using H1299 cells with knock down of SRSF1 or control combined with or without IR treatment. Images of the whole plate are shown. Three experiments were conducted with mean ± SD of relative colony numbers plotted. (d) Growth curve assays were performed using H1299 cells with depletion of SRSF1 or control with or without IR. Three experiments were carried out with mean ± SD of relative cell numbers plotted. (e) Apoptosis of H1299 cells with downregulation of SRSF1 or control combined with or without IR were evaluated by flow cytometry. Three experiments were conducted with mean ± SD of apoptotic cells plotted. (f) Clonogenic survival was examined in colony formation assays in H1299 cells with knock down of SRSF1 or control treated with different dosages of IR. Three experiments were performed with corresponding data normalized to each control and expressed as mean ± SD. (g) SRSF1 knockdown and control cells were fixed at different times after IR (at 0, and 2 h). Immunofluorescence staining for γ-H2AX followed by confocal microscopy was performed to analyze γ-H2AX foci after IR. Cells displaying >10 foci were counted as positive and 300 cells were counted. Representative images of γH2AX foci and the percentage of SRSF1 knockdown and control cells displaying γH2AX foci were shown. Scale bar = 50 μm. (h) Western blot was performed to measure the levels of p-Chk2 and γ-H2AX in H1299 cells with knockdown of SRSF1 upon IR. (i) Comet assay of SRSF1 knockdown and control H1299 cells upon IR. Comet images of DSBs detected by single cell gel electrophoresis at 0.5 h after IR are shown. The tail moment was used as the endpoint of DSBs. 100 individual comets were counted per time point for each experiment. The tail moments were measured and data were represented as the mean tail moment from 3 independent experiments. Data are shown as mean values ± S.D. from three independent experiments. For all panels "*" indicates $p < 0.05$.

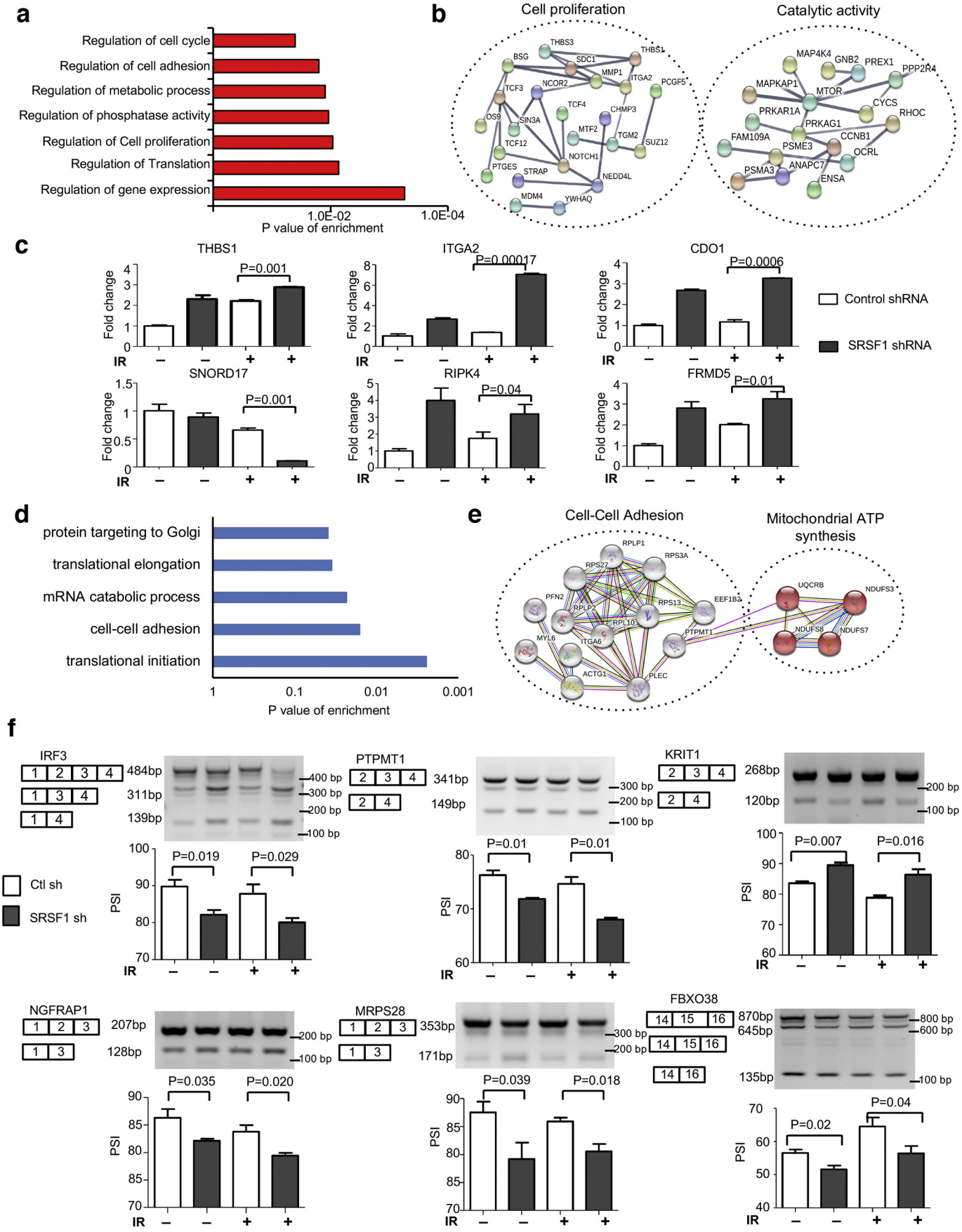
a
Regulation of cell cycle
Regulation of cell adhesion
Regulation of metabolic process
Regulation of phosphatase activity
Regulation of Cell proliferation
Regulation of Translation
Regulation of gene expression
1.0E-02
1.0E-04
P value of enrichment
b
Cell proliferation
Catalytic activity
c
THBS1
ITGA2
CDO1
SNORD17
RIPK4
FRMD5
P=0.001
P=0.00017
P=0.0006
P=0.001
P=0.04
P=0.01
Fold change
IR
Control shRNA
SRSF1 shRNA
d
protein targeting to Golgi
translational elongation
mRNA catabolic process
cell-cell adhesion
translational initiation
1
0.1
0.01
0.001
P value of enrichment
e
Cell-Cell Adhesion
Mitochondrial ATP synthesis
f
IRF3
PTPMT1
KRIT1
NGFRAP1
MRPS28
FBXO38
Ctl sh
SRSF1 sh
PSI
P=0.019
P=0.029
P=0.01
P=0.01
P=0.007
P=0.016
P=0.035
P=0.020
P=0.039
P=0.018
P=0.02
P=0.04

libraries were generated with the rRNA-depleted RNA by NEBNext Ultra™ Directional RNA Library Prep Kits (NEB, USA) according to the manufacturer's protocol. The RNA-seq experiments were performed by Novogene. The RNA-seq dataset was deposited to the Gene Expression Omnibus with accession number GSE107224.

To estimate the gene expression levels, RSEM package and bowtie2 (Li and Dewey, 2011) (Langmead and Salzberg, 2012) were used to align all reads to human reference genome (UCSC hg19 version). To calculate transcript expression levels, we provided a fragment length distribution with options of "–fragment-length-mean 75" and "–fragment-length-sd 10". Subsequently EBSeq tool (Leng, et al., 2013) were used to examine differential expression genes of pairwise comparison according to empirical Bayesian methods.

We mapped the paired-end sequences to human genome (hg19) using MapSplice 2.0.1.6 (default parameters) to discover splicing junctions. To calculate the level of gene expression, we further analyzed the mapped reads using Cufflinks. Then we used MISO package with the annotation of all known alternative splicing events [34] to analyze the change of splicing isoforms, and we filtered the results based on the PSI (percent spliced in) values.

We performed gene ontology enrichment analysis using DAVID GO analysis software to search for enriched pathways. We also analyzed the functional association of SRSF1 targets using protein interaction data from STRING database, generating a set of functional interaction networks. The sub-network containing more than five nodes were demonstrated.

2.14. RNA immunoprecipitation

H1299 cells expressing Flag-SRSF1 or control vector are harvested by trypsinization and resuspended in 10 mL PBS. Formaldehyde (37% stock) is added to the cells to a final concentration of 1% and incubated at room temperature for 10 min with slow rotating. Crosslinking reactions are blocked by the addition of glycine solution (pH 7.0) to a final concentration of 0.25 M followed by incubation at RT for 5 min. After two washes with ice-cold PBS, the cells are collected by centrifugation at 3000 rpm for 4 min at 4 °C and resuspended in 2 mL of RIPA buffer (50 mM Tris-Cl, pH 7.5, 1% NP-40, 0.5% sodium deoxycholate, 0.05% SDS, 1 mM EDTA, 150 mM NaCl) containing protease inhibitors. After three rounds of sonication, solubilized cell lysate was precleared by mixing with M2-Flag beads along with nonspecific tRNA, and collected for immunoprecipitation. The precleared lysate was diluted with RIPA buffer, and immunoprecipitated by incubating with M2-Flag beads for 60–90 min, followed by five or six times washes with 1 mL of RIPA buffer (50 mM Tris-Cl, pH 7.5, 1% NP-40, 1% sodium deoxycholate, 0.1% SDS, 1 mM EDTA, 1 M NaCl, 1 M Urea, 0.2 mM PMSF). The beads were resuspended in 100 μL of 50 mM Tris-Cl, pH 7.0, 5 mM EDTA, 10 mM dithiothreitol (DTT) and 1% SDS and incubated at 70 °C for 45 min to reverse the crosslinks. The RNA was extracted with Trizol following the manufacturer's protocol, and reverse transcribed into cDNA for PCR detection.

2.15. Comet assay

Cells were collected, suspended in PBS at 1×10^5. Mix 25 μL cell suspension with 75 μL Low melting point agarose spread onto a normal melting point agarose-coated slid. After the agarose solidified, the slides were placed in Lysing solution(2.5 mol/L NaCl,100 mmol/L EDTA-Na^2,10 mmol/L tris, 1% Triton X-100 and 10% DMSO) for 2 h. The slides were then subjected to electrophoresis at 25 V and 300.0 mA for 20 min. After electrophoresis, drain the slides on tissue paper and flood with buffer for 3 times, each time 5 min. Cells were stained with DAPI and measured in a fluorescent microscope.

2.16. Immunofluorescence staining

Transfected cells with appropriate density were fixed on the coverslips with 4% paraformaldehyde in 1× PBS for 15 min at room temperature and washed with 1× PBS three times. Cells were then permeabilized with 0.2% Triton X-100 for 10 min and washed with 1 × PBS three times. After blocking in 3% BSA for 30 min, slides were incubated with indicated antibodies (p-H2AX, SRSF1, or HA, 1:100 dilution) antibody diluted in 3% BSA for 2 h. Subsequently, slides were rinsed three times with 1× PBS for 5 min each and then incubated with fluorophore-conjugated secondary antibodies for 1 h. The cover slips were then washed with 1× PBS for three times and mounted with mounting medium (Vector shield's mounting medium with DAPI). Cells were visualized using an Olympus fluorescence microscope, and photographs were captured using a Kodak digital camera.

2.17. Statistics

Student's *t*-test was used for statistical analyses of colony formation, soft agar, and splicing changes.

2.18. Data availability

RNA-seq data in this study have been deposited in Gene Expression Omnibus of NCBI with the accession code GSE107224. The authors declare that all the data supporting the findings of this study are available within the article and its Supplemental information files.

2.19. Study approval

The Institutional Animal Care and Use Committee of the Dalian Medical University approved use of animal models in this study. Informed consent was taken from patients or their guardians prior to participation in the study. Approved use of the tumor specimens in this study was obtained from the Institutional Review Board of the Dalian Medical University.

3. Results

3.1. SRSF1 regulates response to irradiation via modulating DNA double-strand break

Radiotherapy is one of the most effective approaches for cancer therapy, however, cancer cells could develop resistance to radiotherapy and the molecular mechanisms underlying this phenomenon remains unclear. Additionally, the role of aberrant splicing in radioresistance is also elusive.

In order to investigate the role of alternative splicing in radioresistance of cancer cells, we analyzed the data from a published gene expression profile for radioresistance related genes (GSE20549) to identify splicing factors involved in this process. Interestingly, we found SRSF1 is one of the top hits among radioresistance related splicing factors, which is elevated in radioresistant cancer cells (Fig. 1a).SRSF1 has been identified as a potential proto-oncogene that modulates

Fig. 2. Global transcriptional identification of genes regulated by SRSF1 after IR. (a) Gene ontology analyses of SRSF1-regulated gene expression events. Fisher exact p values were plotted for each category. (b) The analyses of functional association networks of SRSF1-regulated genes were performed using the STRING database, with subgroups marked by their functions. (c) The identified gene expression changes were validated by qRT-PCR. The mean ± SD of relative fold changes from triplicate experiments were plotted with p values calculated by paired *t*-test. (d) GO analyses of SRSF1-regulated AS events. Fisher exact p values were plotted for each category. (e) Analysis of functional association networks of SRSF1-regulated AS events were performed using the STRING database, with subgroups marked by their functions. (f) Selected AS events were validated by RT-PCR. The mean ± SD of relative PSI changes from triplicate experiments were plotted with p values calculated by paired t-test.

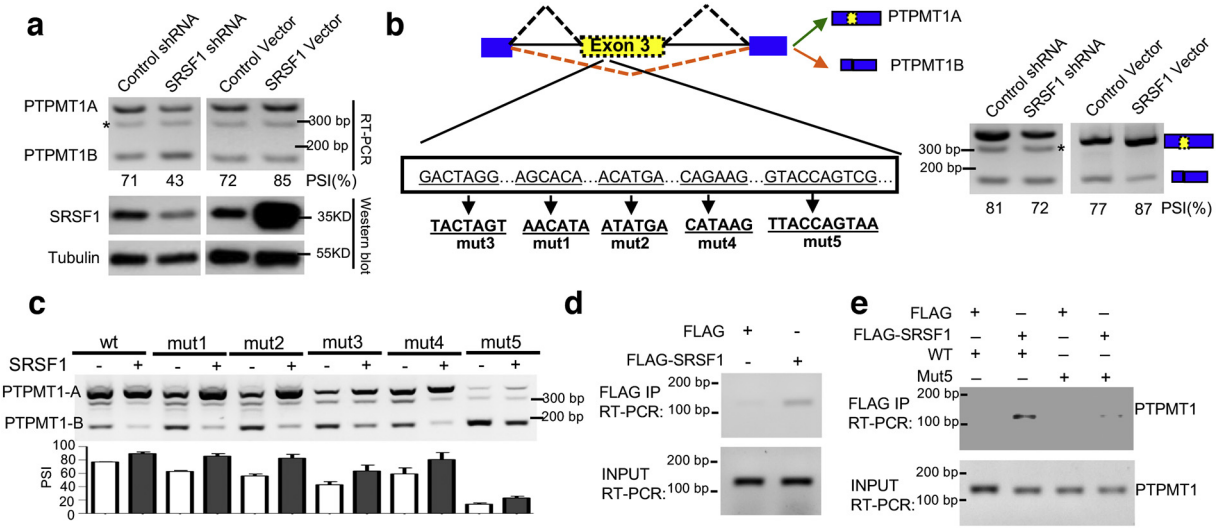

Fig. 3. SRSF1 regulates the AS of PTPMT1. (a) The splicing of PTPMT1 was measured with RT-PCR in H1299 cells with knock down of SRSF1 or control, and H1299 cells overexpressing SRSF1 or control. The level of SRSF1 was evaluated by western blot. (b) A schematic of PTPMT1 pre-mRNA where the potential SRSF1-binding sites are labelled. PTPMT1 splicing reporters with the indicated mutations (mut1 to 5) were generated. The splicing of the wild type PTPMT1 reporter were measured in H1299 cells with knock down of SRSF1or control, and in H1299 cells overexpressing SRSF1 or control vector, using RT-PCR. (c) PTPMT1 splicing reporters containing various mutations were co-expressed with SRSF1 or control in H1299 cells to assay splicing change in PTPMT1. The mean ± SD of PSI was plotted. A representative gel from triplicate experiments was shown. (d) Binding of PTPMT1 pre-mRNAs with SRSF1 is detected by RNA-IP assay in cells exogenously expression FLAG-SRSF1 or control. (e) H1299 cells were co-transfected with Flag-SRSF1 or control and the indicated mutant or wild-type (WT) PTPMT1 reporters, and then immunoprecipitated with anti-Flag antibody. The co-precipitated RNAs were detected by RT-PCR.'*' indicated a non-specific band.

splicing of some cancer associated genes. Meanwhile, increased SRSF1 confers resistance to chemotherapy on cancer cells [35]. Consistently, the levels of SRSF1 were elevated after ionizing radiation (IR) treatment in both H1299 and A549 cells (Fig. 1b), suggesting that SRSF1 might be involved in the radioresistance of lung cancer cells. To further test this possibility, we stably knocked down SRSF1 in NSCLC cells and examined whether the reduction of SRSF1 could affect cell viability after IR (Fig. S1a).Strikingly, downregulation of SRSF1 inhibited clonogenic survival of lung cancer cells after IR treatment as compared to control in two different NSCLC cell lines (H1299 and A549) (Fig. 1c–d and Fig. S1b–c).

Ionizing radiation induces apoptosis in cancer cells. We found that lung cancer cells with decreased SRSF1 displayed a significantly elevated rate of apoptosis compared to controls, particularly upon IR (Fig. 1e and Fig. S1d).Moreover, colony formation assays confirmed that inhibition of SRSF1 significantly increased the sensitivity to IR in two tested lung cancer cell lines (Fig. 1f and Fig. S1e).

To better understand the detailed mechanisms underlying SRSF1-induced radioresistance in lung cancer cells, we measured γH2AX foci formation (indicative of double-strand breaks) [36] by immunofluorescence staining after IR.As shown in Fig. 1g and Fig. S1f, the number of γH2AX foci in SRSF1 knockdown cells were markedly increased, indicating an elevated degree of DNA damage in these cells compared to that in control cells. Meanwhile, the expression level of p-Chk2, another DNA double-strand break marker, was also evidently induced in SRSF1 knockdown cells after IR compared to control (Fig. 1h).Further evaluation of DNA double-strand breaks using COMET assays revealed a significant increase in DNA damage in SRSF1 knockdown cells upon irradiation (Fig. 1i and Fig. S1g).Altogether, our data suggest that loss of SRSF1 may lead to radiosensitization through enhancing DNA double-strand break.

3.2. Global transcriptional identification of genes regulated by SRSF1 after IR

To mechanistically study how SRSF1 impacts tumorigenesis in response to IR, we examined the transcriptomes of control and SRSF1 stably knocking down H1299 cells treated with or without IR by RNA-seq (Fig. S2a). We further applied gene ontology analysis, and found that these genes are significantly associated with cancer related functions, including cell cycle regulation, cell adhesion, cell proliferation and regulation of gene expression (Fig. 2a).

We next performed network analysis using the STRING database to evaluate the interaction of these responsive transcripts (Fig. 2b). Strikingly, the gene-set form a densely-connected network, and one of the largest clusters of genes contains some key regulators of cell proliferation (e.g., NOTCH1, TGM2, and so on). In addition, these genes also include components of signaling pathways that affect catalytic activity (e.g., MAP4K4, MTOR, and so on).

Subsequently, we randomly selected six cancer-related target genes, and tested the RNA-seq results with qRT-PCR. As expected, these events can be validated in both H1299 and A549 cells (Fig. 2c and Fig. S2b).

Next we sought to determine the SRSF1-regulated AS events that may play vital roles in modulating the radioresistance of cancer cells. We identified 42 SRSF1-regulated AS events with an obvious change of percent-spliced-in (PSI) that were overlapped in samples with or without IR treatment (Fig. S2c).When analyzing cellular functions of SRSF1-regulated AS events that differentially expressed after IR, we utilized gene ontology approach and found that after IR,SRSF1 affects genes in RNA processing pathway including translational initiation, mRNA catabolic process, and translational elongation (Fig. 2d). Intriguingly, SRSF1 targeted genes are enriched with tumorigenesis-related functions such as cell-cell adhesion (Fig. 2d). In addition, the majority of SRSF1-controlled AS events were functionally connected into well-linked interaction networks (Fig. 2e). Two of the large subgroups of SRSF1 targets include genes in cell-cell adhesion and mitochondrial ATP synthesis (Fig. 2e). Taken together, these data imply the biological processes influenced by SRSF1 after IR are highly associated with cell proliferation, cell adhesion, and mitochondrial functions.

We further validated the RNA-seq results by determining splicing changes for 6 identified targets, which were arbitrarily selected to include genes with cancer related function. We used two cell lines (H1299 and A549), and confirmed that SRSF1 regulates all tested endogenous AS events, including splicing of IRF3, PTPMT1, NGFRAP1, MRPS28, KRIT1, and FBXO38 (Fig. 2f and Fig. S2d). Together, our results suggest that SRSF1 may modulate the radiosensitivity of cancer cells through controlling AS of cancer related genes.

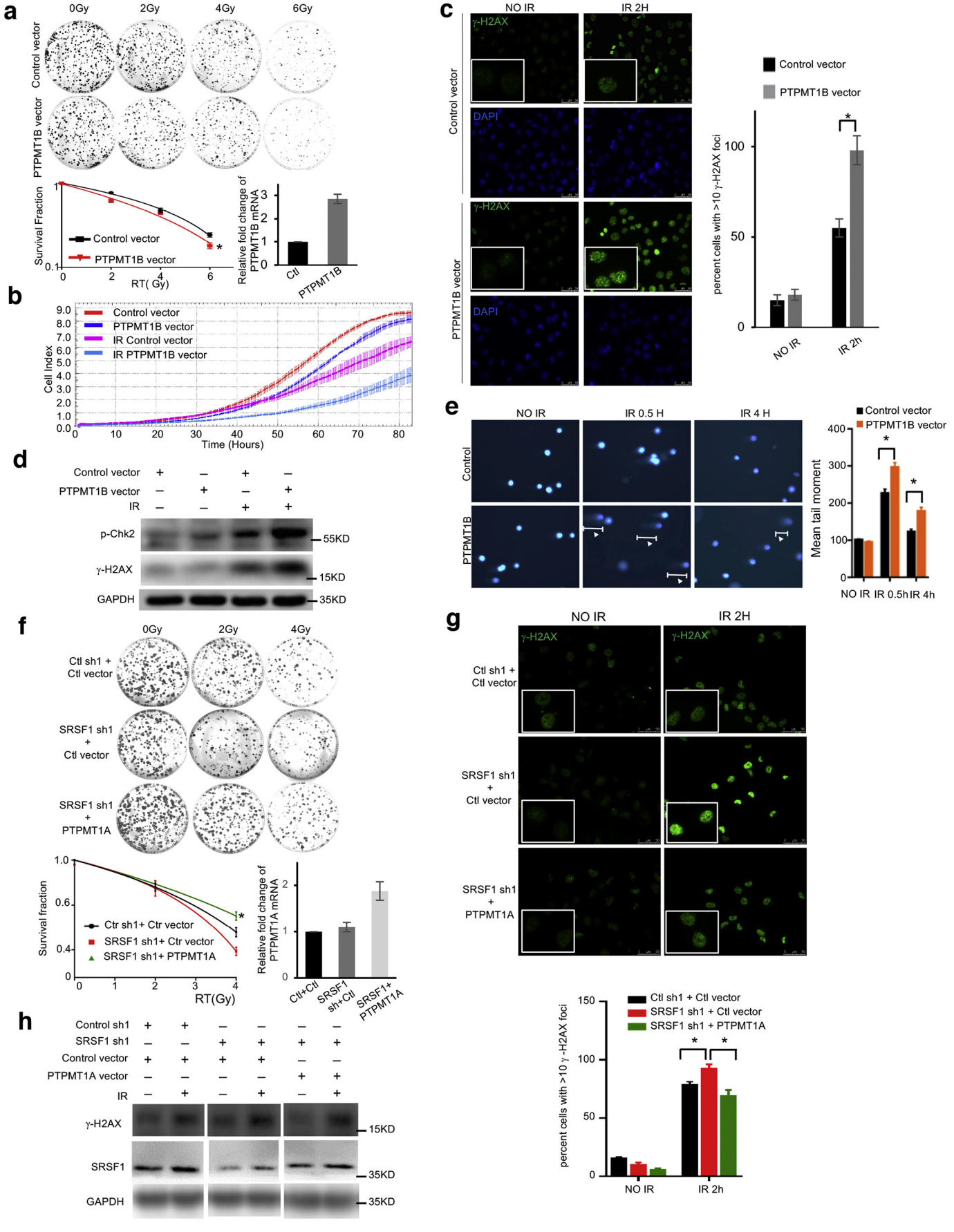
a
0Gy
2Gy
4Gy
6Gy
Control vector
PTPMT1B vector
Survival Fraction
RT(Gy)
Control vector
PTPMT1B vector
Relative fold change of PTPMT1B mRNA
Ctl
PTPMT1B
b
Control vector
PTPMT1B vector
IR Control vector
IR PTPMT1B vector
Cell Index
Time (Hours)
c
NO IR
IR 2H
γ-H2AX
DAPI
Control vector
PTPMT1B vector
Control vector
PTPMT1B vector
percent cells with >10 γ-H2AX foci
NO IR
IR 2h
d
Control vector
PTPMT1B vector
IR
p-Chk2
γ-H2AX
GAPDH
55KD
15KD
35KD
e
NO IR
IR 0.5 H
IR 4 H
Control
PTPMT1B
Control vector
PTPMT1B vector
Mean tail moment
NO IR
IR 0.5h
IR 4h
f
0Gy
2Gy
4Gy
Ctl sh1 + Ctl vector
SRSF1 sh1 + Ctl vector
SRSF1 sh1 + PTPMT1A
Survival fraction
RT(Gy)
Ctr sh1+ Ctr vector
SRSF1 sh1+ Ctr vector
SRSF1 sh1+ PTPMT1A
Relative fold change of PTPMT1A mRNA
Ctl+Ctl
SRSF1 sh+Ctl
SRSF1+ PTPMT1A
g
NO IR
IR 2H
γ-H2AX
Ctl sh1 + Ctl vector
SRSF1 sh1 + Ctl vector
SRSF1 sh1 + PTPMT1A
Ctl sh1 + Ctl vector
SRSF1 sh1 + Ctl vector
SRSF1 sh1 + PTPMT1A
percent cells with >10 γ-H2AX foci
NO IR
IR 2h
h
Control sh1
SRSF1 sh1
Control vector
PTPMT1A vector
IR
γ-H2AX
SRSF1
GAPDH
15KD
35KD
35KD

3.3. SRSF1 regulates the splicing of PTPMT1

Since mitochondrial ATP synthesis is one of the key biological processes affected by SRSF1 after IR. We focused on PTPMT1, a PTEN-like mitochondrial phosphatase, whose splicing has been significantly affected upon depletion of SRSF1 after irradiation.PTPMT1 has two splicing isoforms, including the canonical full-length A isoform and a short B isoform without exon 3 (Fig. S3a).To investigate whether SRSF1 regulates PTPMT1 splicing, we tested if changes of SRSF1 expression could affect PTPMT1 splicing. We found that depletion of SRSF1 shifts the full-length PTPMT1A towards the short isoform PTPMT1B in both H1299 and 293T cells (Fig. 3a and Fig. S3b–c).Conversely, overexpression of SRSF1 switched the splicing to PTPMT1A (Fig. 3a and Fig. S3c). Further analyses revealed that these two PTPMT1 isoforms have similar subcellular localizations, with both PTPMT1A and PTPMT1B are primarily located in the cytoplasm (Fig. S3d). Therefore, SRSF1 is able to regulate the splicing of PTPMT1.

We next examined if SRSF1 directly regulates the splicing of PTPMT1. Bioinformatics analyses(ESE Finder) identified several potential SRSF1 binding sites within the alternatively spliced exon 3 of PTPMT1 (Fig. 3b), suggesting that SRSF1 may regulate splicing through directly binding to PTPMT1 pre-mRNA. To test this possibility, we generated a splicing reporter containing PTPMT1 pre-mRNA with predicted SRSF1 binding sites (Fig. 3b and Fig. S3e) [37]. Consistent with results of the endogenous transcript, knockdown of SRSF1 shifted the splicing of wild-type reporter from PTPMT1A to PTPMT1B (PSI changed from 81% to 72%) (Fig. 3b), and overexpression of SRSF1 switched the splicing towards PTPMT1A (PSI changed from 77% to 87%) (Fig. 3b).

To directly test the role of these potential SRSF1 binding sites in SRSF1- mediated PTPMT1 splicing, we generated multiple splicing reporters containing mutations of the potential SRSF1 binding sites (Fig. 3b). Interestingly, although individual mutants that bear mutations on four of these predicted SRSF1 binding sites failed to alter the splicing of PTPMT1 (Fig. 3C, mut1 to mut4), mutations on the GTACCAGTCG site (mut 5)partially abolished the SRSF1-mediated splicing of PTPMT1, indicating that the potential binding motif is partially responsible for the PTPMT1 splicing switch (Fig. 3c).In addition, by using an RNA-IP approach, we found that SRSF1 does specifically bind to the endogenous PTPMT1 pre-mRNA (Fig. 3d).Further RNA-IP assays with wild type or mutated reporters showed that the SRSF1 binding is indeed dependent on the GTACCAGTCG site, as mutation of this site almost completely prevented the interaction of SRSF1 with the PTPMT1 pre-mRNA (Fig. 3e and Fig. S3f). Collectively, our data demonstrate that SRSF1 directly binds to the alternative exon region of PTPMT1 to control its splicing.

3.4. PTPMT1 splicing switch sensitizes lung cancer cells to IR

To study whether SRSF1-mediated splicing of PTPMT1 contributes to the increased radiosensitivity of cancer cells upon SRSF1 knockdown, we evaluated the impact of the splicing switch, which favors the production of PTPMT1B, on radioresistance of cancer cells. We generated H1299 cells stably expressing PTPMT1B, and the overexpressed PTPMT1B level was about 2.8-fold change as compared to control as judged by realtime RT-PCR, suggesting that the overexpressed PTPMT1B level is similar to the level of PTPMT1B that can be achieved by SRSF1-manipulated splicing (Fig. 4a).We further applied colony formation assays after different dosages of IR to analyze the relationship between PTPMT1B and the cellular response to IR. Remarkably, lung cancer cells stably expressing PTPMT1B significantly increased sensitivity to IR as compared to control (Fig. 4a). Moreover, PTPMT1B displayed a substantially enhanced ability to inhibit cancer cell proliferation than control, particularly when cells were treated with IR (Fig. 4b), and PTPMT1B induced elevated DNA damage upon IR compared to control (Fig. 4c).Consistently, the level of Chk2 and γH2AX were dramatically increased by PTPMT1B after IR (Fig. 4d). COMET assays also confirmed that cells expressing PTPMT1B had increased DNA double-strand breaks upon IR compared to control (Fig. 4e). Similarly, we found that specific knockdown of PTPMT1A significantly inhibited cancer cell growth, especially upon ionizing treatment (Fig. S4a–c). Conversely, re-expression of PTPMT1A in SRSF1 knocking-down cells significantly inhibited DNA damage upon IR (Fig. 4f–h and Fig. S4d).Taken together, our results indicate that the splicing switch of PTPMT1 can sensitize cancer cells to IR and suggest that depletion of SRSF1 sensitizes cancer cells to radiotherapy through increased splicing of PTPMT1B.

3.5. PTPMT1 splicing induces the expression of p-AMPK to increase radiosensitivity

To further evaluate the importance of SRSF1-mediated PTPMT1 splicing in regulating the radiosensitivity of cancer cells, we dissected the possible molecular mechanisms underlying this axis of SRSF1-PTPMT1. It has been previously reported that AMPK was highly activated in PTPMT1 knockout cells [38]. Importantly, we found that the p-AMPK level was markedly elevated upon IR in SRSF1 knockdown cells as compared to control (Fig. 5a).Consistently, upon irradiation, PTPMT1B overexpressed cells demonstrated an evidently increased p-AMPK level, as well as the corresponding changes of its downstream targets, including elevated p21 and p27 levels, and decreased p-mTOR level (Fig. 5b).

Further clonogenic survival assays revealed that knockdown of AMPK in SRSF1-depleted cells reversed the radiosensitization of cancer cells, as reduced levels of AMPK in SRSF1 knockdown cells promoted the survival of cells, thereby conferring the cancer cells radioresistance (Fig. 5c). Moreover, the decreased level of AMPK can also significantly inhibit DNA double-strand break in SRSF1 knockdown cells when treated with IR (Fig. 5d and e).

3.6. PTPMT1 splicing induces radiosensitivity in vivo and is correlated with survival

To directly test whether SRSF1 knockdown increases radiosensitivity through regulating PTPMT1 splicing in vivo, we treated nude mice bearing xenografts from H1299-PTPMT1B, or H1299-control with or without IR. Strikingly, overexpression of PTPMT1B combined with IR significantly suppressed tumor growth (Fig. 6a–c). In addition, the

Fig. 4. PTPMT1 splicing switch induces DNA damage. (a) Clonogenic survival was examined in colony formation assays in H1299 cells with ectopic expression of PTPMT1B or control treated with different dosages of IR. The mRNA expression levels of PTPMT1B were examined with realtime RT-PCR. Three experiments were carried out with corresponding data normalized to each control and expressed as mean ± SD (* indicated $p < 0.05$). (b) Growth curve assays were performed to evaluate the proliferation of H1299 cells overexpressing PTPMT1B or control that were treated with or without IR. (c) H1299 cells with ectopic expression of PTPMT1B or control were fixed at different times after IR (at 0, and 2 h). Immunofluorescence assay for γ-H2AX followed by confocal microscopy was performed to evaluate γ-H2AX foci at different times after IR. Representative images of γ-H2AX foci and the percentage of ectopic expression of PTPMT1B and control cells displaying γ-H2AX foci were shown. Scale bar = 50 μm. (d) Western blot was used to examine the levels of p-Chk2 and γ-H2AX in H1299 cells with ectopic expression of PTPMT1B or control upon IR. (e) Comet assay of H1299 cells with expression of PTPMT1B or control upon IR. Comet images of DSBs detected by single cell gel electrophoresis at 0.5 h after IR are shown. Data are shown as mean values ± S.D. from three independent experiments. (f) Clonogenic survival was determined in colony formation assays in H1299 cells with knocking down SRSF1 or control, and re-expressing PTPMT1A in SRSF1 depleted condition, which were treated with different dosages of IR. The mRNA expression levels of PTPMT1A were examined with realtime RT-PCR. Three experiments were performed with corresponding data normalized to each control and expressed as mean ± SD. (g) H1299 cells with depletion of SRSF1 or control, and re-expression of PTPMT1A in SRSF1 depleted status were fixed at different times after IR (at 0 and 2 h) and immuno-stained for γ-H2AX foci. Representative images of γ-H2AX foci and the percentage of cells displaying γ-H2AX foci are shown. Scale bar = 50 μm. (h) Western blot was applied to determine the levels of γ-H2AX in H1299 cells with depletion of SRSF1 or control, and re-expression of PTPMT1A in SRSF1 depleted status with or without IR. For all panels "*" indicated $p < 0.05$.

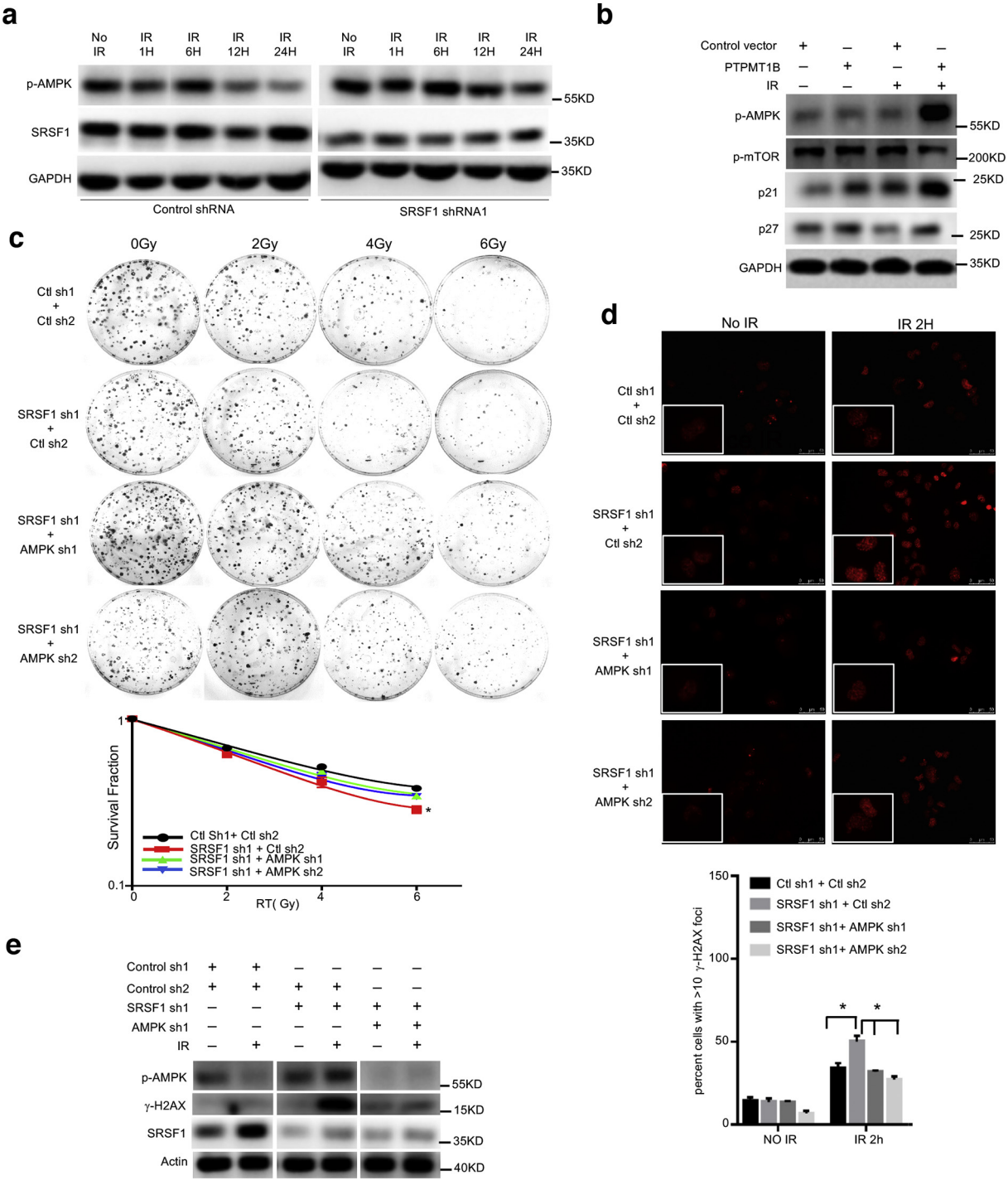

Fig. 5. PTPMT1 splicing induces the expression of p-AMPK to increase radiosensitivity. (a) Western blots were performed to examine the protein levels of p-AMPK in H1299 cells with knockdown of SRSF1 or control at 0, 1, 6, 12, 24 h after IR. (b) The protein levels of p-AMPK and its downstream targets were measured in H1299 cell with ectopic expression of PTPMT1B or control. (c) Clonogenic survival was examined in colony formation assays in H1299 cells stably expressing SRSF1 sh1 and control sh2, SRSF1 sh1 and AMPK sh1, SRSF1 sh1 and AMPK sh2, or control sh1 and control sh2 treated with different dosages of IR. Three experiments were carried out with corresponding data normalized to each control and expressed as mean ± SD. (d) H1299 cells stably expressing SRSF1 sh1 and control sh2, SRSF1 sh1 and AMPK sh1, SRSF1 sh1 and AMPK sh2, or control sh1 and control sh2 were fixed at different times after IR (at 0, and 2 h) and immuno-stained for γ-H2AX foci. Representative images of γ-H2AX foci and the percentage of cells displaying γ-H2AX foci are shown. Scale bar = 50 μm. (e) Western blot was used to test the levels of p-AMPK and γ-H2AX in H1299 cells stably expressing SRSF1 sh1 and control sh2, SRSF1 sh1 and AMPK sh1, or control sh1 and control sh2, which were treated with or without IR. For all panels "*" indicated $p < 0.05$.

levels of p-AMPK and γ-H2AX were evidently increased in PTPMT1B-expressing xenografts upon IR (Fig. 6d), suggesting that PTPMT1 splicing does induce DNA damage to sensitize cancer cells to radiotherapy in vivo.

To further test the clinical significance of SRSF1-regulated splicing of PTPMT1 in cancer patients, we examined the relative levels of two PTPMT1 isoforms in paired NSCLC samples and adjacent normal tissues surgically collected from 6 patients. Compared to the paired normal tissues, the relative mRNA levels of PTPMT1B were substantially decreased in all tested primary NSCLC specimens (Fig. 6e) that had elevated expression of SRSF1 (Fig.S5a–b), suggesting a common decrease of PTPMT1B expression despite obvious heterogeneity in different tumor

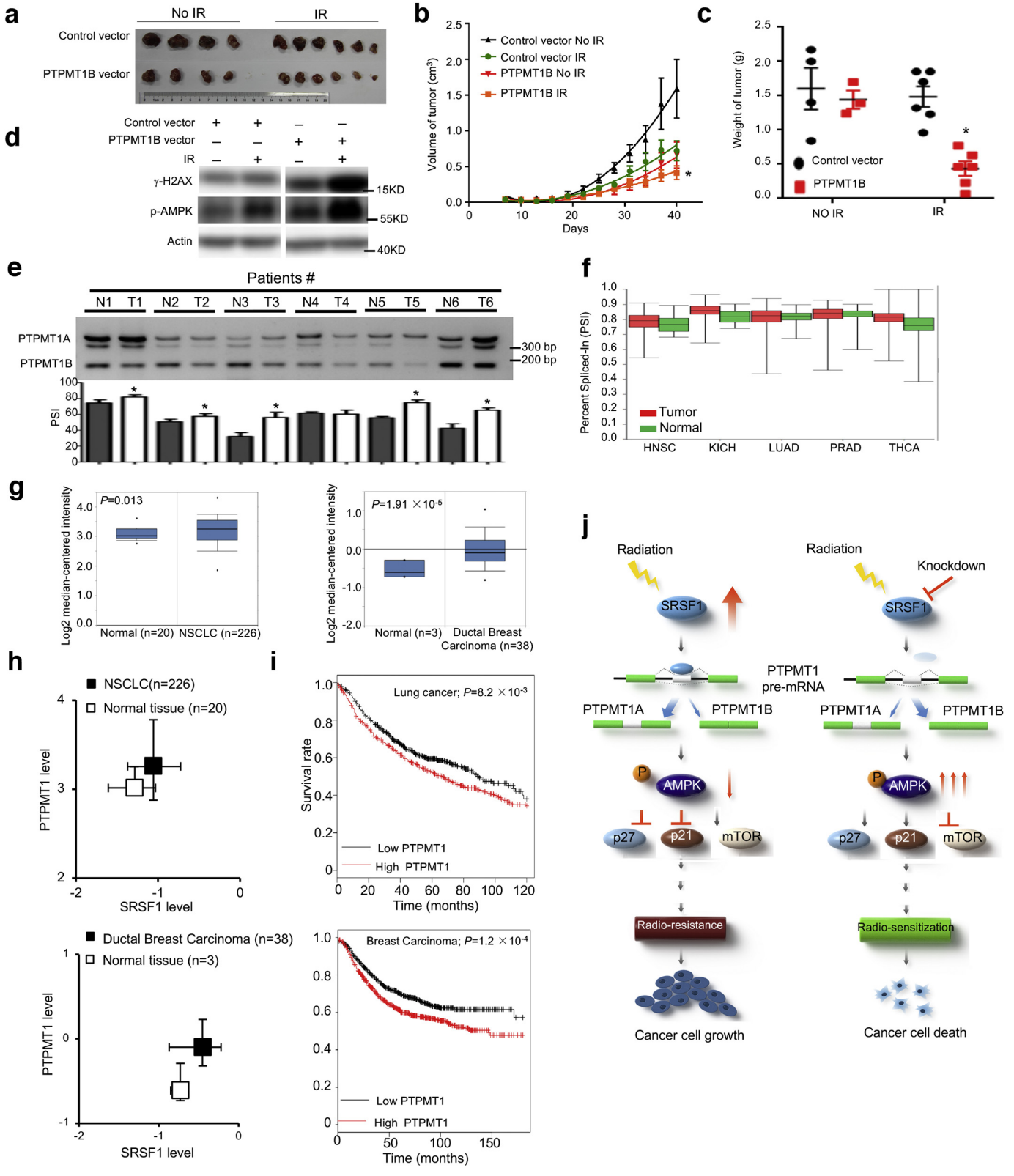

specimens. In support of our observations, analyses of RNA-seq datasets from the TCGA consortium indicated that PTPMT1B levels were dramatically decreased in 5 tumor types, including lung, head and neck, renal, prostate and thyroid cancer (Fig. 6f).

We subsequently analyzed the datasets from large scale studies [39–45], and found the level of PTPMT1A is significantly elevated in lung and breast cancers (Fig. 6g), which is positively correlated to SRSF1 level (Fig. 6h). In addition, we used Kaplan-Meier Plotter to evaluate the overall survival of cancer patients with different PTPMT1A levels using datasets from large scale screening [46]. As expected, higher expression of PTPMT1A was related to poor overall survival in patients with lung and breast cancer (Fig. 6i).

4. Discussion

Radioresistance may lead to cancer recurrence and poor prognosis. Many factors play vital roles in radioresistance. It has been reported that EGFR overexpression is closely correlated to irradiation resistance, thus the application of EGFR inhibitor can sensitize cancer cells to radiotherapy [47–49]. In addition, activation of NF-kappa B is associated with radioresistance in several kinds of cancers [50], whereas inhibition of NF-kappa B improves sensitivity to irradiation [51]. αvβ3 integrin can also mediates radioresistance of prostate cancer cells through regulation of survivin [52]. Interestingly, radiation-activated CDC6 protein stability results in radioresistance via mediating senescence and EMT [53].

Deregulation of AS is one of most important molecular hallmarks of cancer [7–10], however the detailed mechanisms and biological consequences are still elusive. Notably, whether aberrant AS plays vital roles in the development of radioresistance in cancer cells remains unknown. Here we report a novel function of SRSF1 in regulating radioresistance of lung cancer cells. Previously, SRSF1 has been shown to control the splicing of RON and BIN1, thus promoting breast cancer progression [26]. In our model, for the first time, we demonstrated that IR can elevate the level of SRSF1, which in turn promote the splicing of PTPMT1 to the long form, thereby reducing the level of p-AMPK. Such decrease inhibits DNA damage, and confers cancer cells to resist to radiotherapy. Conversely, when the level of SRSF1 is decreased, it can switch the splicing of PTPMT1 towards PTPMT1B. Strikingly, such splicing switch elevates the level of p-AMPK, thus induces DNA double strand break, and sensitizes lung cancer cells to radiotherapy (Fig. 6j). Altogether our results represent a novel mechanism for how SRSF1 is involved in radioresistance through modulating AS of new cancer related genes.

SRSF1 is a well-known splicing factor that can promote tumorigenesis via regulating alternative splicing, however, in addition to splicing regulation, it has been previously reported that SRSF1 interacts with translating ribosomes and promotes translation [23].By analyzing the RNA-seq data, we found that translation regulation was also enriched in the gene ontology analyses upon SRSF1 knockdown, suggesting that SRSF1 may also contribute to radioresistance of cancer cells by regulating translation initiation and elongation.

Intriguingly, our data suggest that PTPMT1B can reduce the clonogenic survival rate of lung cancer cells after IR. Consistently, the level of PTPMT1B is reduced in lung cancer patients' samples. In addition, analyses of TCGA datasets also suggest that the splicing of PTPMT1 is frequently changed in several cancer patients to decrease PTPMT1B. Re-expression of PTPMT1B markedly elevated the level of p-AMPK, thus inducing the DNA double-strand breaks. Therefore, manipulating PTPMT1 splicing may provide a novel approach to sensitize cancer cells to radiotherapy. Particularly, PTPMT1 splicing is regulated by SRSF1, an oncogenic splicing factor. Loss of SRSF1 increases the production of PTPMT1B, which might in turn sensitize cancer cells to IR through distinct signaling pathway.

However, the splicing of PTPMT1 towards the short isoform may not account for the radiosensitization totally. Other SRSF1-controlled splicing events might also contribute the radioresistance of cancer cells. Using RNA-seq, we also found that SRSF1 regulated some AS events of genes associated with cell-cell adhesion and mitochondrial ATP synthesis. For instance, SRSF1 controls splicing of MRPS28, which has been demonstrated to participate in response to IR in a cervical cancer cell line [54]. These data indicate that SRSF1 modulates many AS events critical to radio-resistance, which may provide a potential therapeutic approach to sensitize cancer cells to radiotherapy. But SRSF1 also has several physiological functions to maintain cells in certain condition. We may not want to completely deplete SRSF1. In this case, we might use antisense oligos to switch the splicing of some key genes, such as PTPMT1 for example. In addition, the application of antisense oligos targeting several genes will provide a more robust effect to sensitize cancer cells to radiotherapy.

Taken together, our data show that reduced SRSF1 mediates the AS of PTPMT1 and other genes, which together may contribute to the sensitization of cancer cells to radiotherapy. >90% of human genes undergo alternative splicing, thus aberrant splicing plays a key role in tumorigenesis, as well as radioresistance of cancer cells to radiotherapy. Therefore, detailed studies of deregulated splicing are important to provide new insights in radioresistance of different cancers. Our study offers acritical example of how a splicing factor can regulate vital AS events in radioresistance of cancer cells, which can be potentially explored as a new route of sensitizing cancer cells to radiotherapy.

5. Conclusions

In summary, we find that SRSF1 regulates lung cancer cell radioresistance through modulating PTPMT1 splicing. Reduced SRSF1 favors the production of short isoforms of PTPMT1 upon ionizing radiation, which in turn promotes phosphorylation of AMPK, thereby inducing DNA double-strand break to sensitize cancer cells to irradiation. Additionally, the level of the short isoforms of PTPMT1 is decreased in cancer samples, which is correlated to cancer patients' survival. Our study provides mechanistic analyses of aberrant splicing in radioresistance in lung cancer cells, and establishes SRSF1 as a potential therapeutic target for sensitization of patients to radiotherapy.

Funding

This work was supported by the National Natural Science Foundation of China (81830088, 81422038, 91540110, and 31471235 to Y.W.; 81872247 and 31400726 to W. Z.; 81402549 to G. Z.); the Department of Science and Technology of Dalian City (the 'Dalian Supports High Level Talents Innovation and Entrepreneurship Program' 2016RJ02 to Y.W.);the Newton Advanced Fellowship from the Academy of Medical Sciences in UK (JXR11831 to Y.W. and J. C.); and the Liaoning S&T Project (2015020301 to W. Z., 2015033 to G. Z.).

Availability of data and materials

All data generated or analyzed during this study are included in this published article and its supplementary information files.

Authors' contributions

Y. W. and W. Z. designed experiments, interpreted the results and wrote the manuscript. B. S., W. Z., J. S., Q. Z., L. B., Q.Y., L. C., Y. L., J. Z., Y.S. and L.Z. performed experiments. Q. L., C. G., X. D., G. Z., J. C., H. L., S. M., X. L. and H. G. help to interpret the data. P.Q. analyzed the RNA-seq and TCGA data.

Fig. 6. PTPMT1 splicing induces radiosensitivity in vivo and is correlated with survival in patient. (a) H1299 cells stably expressing PTPMT1B or control were subcutaneously injected into the flank of nude mice respectively. Mice were subsequently treated with or without 6 Gy IR. Pictures of the tumors removed after 40 days were shown. (b) The average sizes of xenograft tumors measured every 5 days (error bars indicate ± SD). (c) The weights of the tumors were examined, and the median, upper and lower quartiles of tumor volume were plotted. (d) Western blot was applied to determine the levels of p-AMPK and γ-H2AX in representative mice tumors from different treatment groups. (e) Total RNAs isolated from 6 paired NSCLC tumors and adjacent normal tissues were assayed to measure the splicing of PTPMT1 by qRT-PCR. The mean ± SD from three experiments was plotted. (f) The splicing alteration of PTPMT1 was examined in various cancers by analyzing the TCGA consortium containing RNA-seq datasets from thousands of patients. (g) PTPMT1A mRNA level in lung and breast cancer. Oncomine was used to analyze previously collected data. The median, upper and lower quartiles were plotted, and the whiskers that extend from each box indicate the range values that were outside of the intra-quartile range. (h) Correlation of PTPMT1A and SRSF1 in lung and breast cancer patients. Oncomine was utilized to evaluate expression data. The mean levels of PTPMT1A and SRSF1 were plotted, error bars indicate upper and lower quartile. (i) Kaplan-Meier curve showing overall survival of patients with lung and breast cancers bearing high or low PTPMT1A expression. (j) The model of how SRSF1 regulates radiosensitivity through modulating AS. For all panels "*" indicated $p < 0.05$.

Competing interests

The authors declare that they have no competing interests.

Consent for publication

We have obtained consents to publish this paper from all the participants of this study.

Ethics approval and consent to participate

The Institutional Animal Care and Use Committee of the Dalian Medical University approved use of animal models in this study.

All human tumor tissues were obtained with written informed consent from patients or their guardians prior to participation in the study. The Institutional Review Board of the Dalian Medical University approved use of the tumor specimens in this study.

Acknowledgements

We thank members of the Wang laboratory for their technical support and discussions throughout the study.

Appendix A. Supplementary data

Supplementary data to this article can be found online at https://doi.org/10.1016/j.ebiom.2018.11.007.

References

[1] Dungey FA, Caldecott KW, Chalmers AJ. Enhanced radiosensitization of human glioma cells by combining inhibition of poly(ADP-ribose) polymerase with inhibition of heat shock protein 90. Mol Cancer Ther 2009;8:2243–54.
[2] Wang YV, Leblanc M, Wade M, Jochemsen AG, Wahl GM. Increased radioresistance and accelerated B cell lymphomas in mice with Mdmx mutations that prevent modifications by DNA-damage-activated kinases. Cancer Cell 2009;16:33–43.
[3] Yin Y, Li R, Xu K, Ding S, Li J, Baek G, et al. Androgen receptor variants mediate DNA repair after prostate cancer irradiation. Cancer Res 2017;77:4745–54.
[4] Yogev O, Barker K, Sikka A, Almeida GS, Hallsworth A, Smith LM, et al. p53 loss in MYC-driven neuroblastoma leads to metabolic adaptations supporting radioresistance. Cancer Res 2016;76:3025–35.
[5] Wang J, Wakeman TP, Lathia JD, Hjelmeland AB, Wang XF, White RR, et al. Notch promotes radioresistance of glioma stem cells. Stem Cells 2010;28:17–28.
[6] Pan Q, Shai O, Lee LJ, Frey BJ, Blencowe BJ. Deep surveying of alternative splicing complexity in the human transcriptome by high-throughput sequencing. Nat Genet 2008;40:1413–5.
[7] Bechara EG, Sebestyen E, Bernardis I, Eyras E, Valcarcel J. RBM5, 6, and 10 differentially regulate NUMB alternative splicing to control cancer cell proliferation. Mol Cell 2013;52:720–33.
[8] Shkreta L, Bell B, Revil T, Venables JP, Prinos P, Elela SA, et al. Cancer-associated perturbations in alternative pre-messenger RNA splicing. Cancer Treat Res 2013;158:41–94.
[9] David CJ, Manley JL. Alternative pre-mRNA splicing regulation in cancer: Pathways and programs unhinged. Genes Dev 2010;24:2343–64.
[10] Venables JP. Aberrant and alternative splicing in cancer. Cancer Res 2004;64:7647–54.
[11] Venables JP, Klinck R, Bramard A, Inkel L, Dufresne-Martin G, Koh C, et al. Identification of alternative splicing markers for breast cancer. Cancer Res 2008;68:9525–31.
[12] Venables JP, Burn J. EASI—enrichment of alternatively spliced isoforms. Nucleic Acids Res 2006;34:e103.
[13] Qi Y, Yu J, Han W, Fan X, Qian H, Wei H, et al. A splicing isoform of TEAD4 attenuates the Hippo-YAP signalling to inhibit tumour proliferation. Nat Commun 2016;7:ncomms11840.
[14] Wang Y, Chen D, Qian H, Tsai YS, Shao S, Liu Q, et al. The splicing factor RBM4 controls apoptosis, proliferation, and migration to suppress tumor progression. Cancer Cell 2014;26:374–89.
[15] Anczukow O, Krainer AR. Splicing-factor alterations in cancers. RNA 2016;22:1285–301.
[16] Dvinge H, Kim E, Abdel-Wahab O, Bradley RK. RNA splicing factors as oncoproteins and tumour suppressors. Nat Rev Cancer 2016;16:413–30.
[17] Erkelenz S, Mueller WF, Evans MS, Busch A, Schoneweis K, Hertel KJ, et al. Position-dependent splicing activation and repression by SR and hnRNP proteins rely on common mechanisms. RNA 2013;19:96–102.
[18] Wang Y, Xiao X, Zhang J, Choudhury R, Robertson A, Li K, et al. A complex network of factors with overlapping affinities represses splicing through intronic elements. Nat Struct Mol Biol 2013;20:36–45.
[19] Das R, Yu J, Zhang Z, Gygi MP, Krainer AR, Gygi SP, et al. SR proteins function in coupling RNAP II transcription to pre-mRNA splicing. Mol Cell 2007;26:867–81.
[20] Michlewski G, Sanford JR, Caceres JF. The splicing factor SF2/ASF regulates translation initiation by enhancing phosphorylation of 4E-BP1. Mol Cell 2008;30:179–89.
[21] Zhang Z, Krainer AR. Involvement of SR proteins in mRNA surveillance. Mol Cell 2004;16:597–607.
[22] Fregoso OI, Das S, Akerman M, Krainer AR. Splicing-factor oncoprotein SRSF1 stabilizes p53 via RPL5 and induces cellular senescence. Mol Cell 2013;50:56–66.
[23] Sanford JR, Gray NK, Beckmann K, Caceres JF. A novel role for shuttling SR proteins in mRNA translation. Genes Dev 2004;18:755–68.
[24] Maslon MM, Heras SR, Bellora N, Eyras E, Caceres JF. The translational landscape of the splicing factor SRSF1 and its role in mitosis. Elife 2014 (3: e02028).
[25] Aznarez I, Nomakuchi TT, Tetenbaum-Novatt J, Rahman MA, Fregoso O, Rees H, et al. Mechanism of nonsense-mediated mRNA decay stimulation by splicing factor SRSF1. Cell Rep 2018;23:2186–98.
[26] Anczukow O, Rosenberg AZ, Akerman M, Das S, Zhan L, Karni R, et al. The splicing factor SRSF1 regulates apoptosis and proliferation to promote mammary epithelial cell transformation. Nat Struct Mol Biol 2012;19:220–8.
[27] Karni R, de Stanchina E, Lowe SW, Sinha R, Mu D, Krainer AR. The gene encoding the splicing factor SF2/ASF is a proto-oncogene. Nat Struct Mol Biol 2007;14:185–93.
[28] Das S, Anczukow O, Akerman M, Krainer AR. Oncogenic splicing factor SRSF1 is a critical transcriptional target of MYC. Cell Rep 2012;1:110–7.
[29] Bonomi S, di Matteo A, Buratti E, Cabianca DS, Baralle FE, Ghigna C, et al. HnRNP A1 controls a splicing regulatory circuit promoting mesenchymal-to-epithelial transition. Nucleic Acids Res 2013;41:8665–79.
[30] de Miguel FJ, Sharma RD, Pajares MJ, Montuenga LM, Rubio A, Pio R. Identification of alternative splicing events regulated by the oncogenic factor SRSF1 in lung cancer. Cancer Res 2014;74:1105–15.
[31] Liu J, Bhadra M, Sinnakannu JR, Yue WL, Tan CW, Rigo F, et al. Overcoming imatinib resistance conferred by the BIM deletion polymorphism in chronic myeloid leukemia with splice-switching antisense oligonucleotides. Oncotarget 2017;8:77567–85.
[32] Clower CV, Chatterjee D, Wang Z, Cantley LC, Vander Heiden MG, Krainer AR. The alternative splicing repressors hnRNP A1/A2 and PTB influence pyruvate kinase isoform expression and cell metabolism. Proc Natl Acad Sci U S A 2010;107:1894–9.
[33] Dehm SM. mRNA splicing variants: Exploiting modularity to outwit cancer therapy. Cancer Res 2013;73:5309–14.
[34] Katz Y, Wang ET, Airoldi EM, Burge CB. Analysis and design of RNA sequencing experiments for identifying isoform regulation. Nat Methods 2010;7:1009–15.
[35] Shultz JC, Goehe RW, Murudkar CS, Wijesinghe DS, Mayton EK, Massiello A, et al. SRSF1 regulates the alternative splicing of caspase 9 via a novel intronic splicing enhancer affecting the chemotherapeutic sensitivity of non-small cell lung cancer cells. Mol Cancer Res 2011;9:889–900.
[36] Firsanov D, Vasilishina A, Kropotov A, Mikhailov V. Dynamics of gammaH2AX formation and elimination in mammalian cells after X-irradiation. Biochimie 2012;94:2416–22.
[37] Cartegni L, Wang J, Zhu Z, Zhang MQ, Krainer AR. ESEfinder: A web resource to identify exonic splicing enhancers. Nucleic Acids Res 2003;31:3568–71.
[38] Yu WM, Liu X, Shen J, Jovanovic O, Pohl EE, Gerson SL, et al. Metabolic regulation by the mitochondrial phosphatase PTPMT1 is required for hematopoietic stem cell differentiation. Cell Stem Cell 2013;12:62–74.
[39] Talbot SG, Estilo C, Maghami E, Sarkaria IS, Pham DK, Oc P, et al. Gene expression profiling allows distinction between primary and metastatic squamous cell carcinomas in the lung. Cancer Res 2005;65:3063–71.
[40] Richardson AL, Wang ZC, De Nicolo A, Lu X, Brown M, Miron A, et al. X chromosomal abnormalities in basal-like human breast cancer. Cancer Cell 2006;9:121–32.
[41] Gumz ML, Zou H, Kreinest PA, Childs AC, Belmonte LS, Legrand SN, et al. Secreted frizzled-related protein 1 loss contributes to tumor phenotype of clear cell renal cell carcinoma. Clin Cancer Res 2007;13:4740–9.
[42] Ki DH, Jeung HC, Park CH, Kang SH, Lee GY, Lee WS, et al. Whole genome analysis for liver metastasis gene signatures in colorectal cancer. Int J Cancer 2007;121:2005–12.
[43] Crabtree JS, Jelinsky SA, Harris HA, Choe SE, Cotreau MM, Kimberland ML, et al. Comparison of human and rat uterine leiomyomata: identification of a dysregulated mammalian target of rapamycin pathway. Cancer Res 2009;69:6171–8.
[44] D'Errico M, de Rinaldis E, Blasi MF, Viti V, Falchetti M, Calcagnile A, et al. Genome-wide expression profile of sporadic gastric cancers with microsatellite instability. Eur J Cancer 2009;45:461–9.
[45] Bonome T, Levine DA, Shih J, Randonovich M, Pise-Masison CA, Bogomolniy F, et al. A gene signature predicting for survival in suboptimally debulked patients with ovarian cancer. Cancer Res 2008;68:5478–86.
[46] Gyorffy B, Lanczky A, Szallasi Z. Implementing an online tool for genome-wide validation of survival-associated biomarkers in ovarian-cancer using microarray data from 1287 patients. Endocr Relat Cancer 2012;19:197–208.
[47] Akimoto T, Hunter NR, Buchmiller L, Mason K, Ang KK, Milas L. Inverse relationship between epidermal growth factor receptor expression and radiocurability of murine carcinomas. Clin Cancer Res 1999;5:2884–90.
[48] Zhou H, Kim YS, Peletier A, McCall W, Earp HS, Sartor CI. Effects of the EGFR/HER2 kinase inhibitor GW572016 on EGFR- and HER2-overexpressing breast cancer cell line proliferation, radiosensitization, and resistance. Int J Radiat Oncol Biol Phys 2004;58:344–52.
[49] Chakravarti A, Dicker A, Mehta M. The contribution of epidermal growth factor receptor (EGFR) signaling pathway to radioresistance in human gliomas: a review of preclinical and correlative clinical data. Int J Radiat Oncol Biol Phys 2004;58:927–31.
[50] Bai M, Ma X, Li X, Wang X, Mei Q, Li X, et al. The accomplices of NF-kappaB lead to radioresistance. Curr Protein Pept Sci 2015;16:279–94.

[51] Wang R, Peng S, Zhang X, Wu Z, Duan H, Yuan Y, et al. Inhibition of NF-kappaB improves sensitivity to irradiation and EGFR-TKIs and decreases irradiation-induced lung toxicity. Int J Cancer 2018. https://doi.org/10.1002/ijc.31907.
[52] Wang T, Huang J, Vue M, Alavian MR, Goel HL, Altieri DC, et al. alphavbeta3 integrin mediates radioresistance of prostate cancer cells through regulation of survivin Mol Cancer Res 2018. https://doi.org/10.1158/1541-7786.MCR-18-0544.
[53] Yu X, Liu Y, Yin L, Peng Y, Peng Y, Gao Y, et al. Radiation-promoted CDC6 protein stability contributes to radioresistance by regulating senescence and epithelial to mesenchymal transition. Oncogene 2018. https://doi.org/10.1038/s41388-018-0460-4.
[54] Gopal G, Rajkumar T. Variant of mitochondrial ribosomal protein s28 (mrps28) gene is differentially expressed in response to radiation in a cervical carcinoma derived cell line. Indian J Biochem Biophys 2005;42:81–6.